IOP Conf. Series: Materials Science and Engineering **228** (2017) 012005 doi:10.1088/1757-899X/228/1/012005

Investigations of fluid flow effects on dendritic solidification: Consequences on fragmentation, macrosegregation and the influence of electromagnetic stirring

N Shevchenko[1,*], H Neumann-Heyme[1], C Pickmann[2], E Schaberger-Zimmermann[3], G Zimmermann[2], K Eckert[1], S Eckert[1]

[1] Helmholtz-Zentrum Dresden-Rossendorf (HZDR), 01328 Dresden, Germany

[2] ACCESS e.V., Intzestrasse 5, 52072 Aachen, Germany

[3] RWTH, Foundry Institute, Intzestrasse 5, 52072 Aachen, Germany

[*] n.shevchenko@hzdr.de

Abstract. Solidification experiments and numerical simulations have been performed to improve the understanding of the complex interrelation between melt flow and the formation of dendritic structures during solidification of Al-Cu and Ga-In alloys. Melt flow induces various effects on grain morphology primarily caused by convective transport of solute, such as a facilitation of the growth of primary trunks or lateral branches, dendrite remelting, fragmentation or freckle formation depending on the dendrite orientation, the flow direction and intensity. Within this project special interest was focused on fragmentation and segregation phenomena. Natural convection is caused by density variations within the solidifying alloys. Forced convection was produced by electromagnetic stirring. X-ray radioscopy was applied as a powerful tool for the visualization of dendritic growth and coarsening.

1. Introduction

Fluid flow plays an important role in solidification processes, since the convective transport of heat and solute influences the undercooling at the solidification front and thus determines the growth conditions of the solid phase decisively. The occurrence of a flow in a solidifying melt must be regarded as the normal case, since natural convection begins once there are significant differences in temperature or composition. In particular, thermo-solutal convection has been identified as the main reason for the development of solute-rich channels in the mushy zone [1-4]. The incidence of such segregation channels in fully-solidified castings has to be considered as a serious casting defect.

A sufficient understanding of the strongly coupled interaction between the melt flow and the solidification requires a detailed knowledge of the velocity field especially in the vicinity of the solidification front. During an upwards solidification solutal convection may arise from an unstable density stratification at the solid-liquid interface if the solute component rejected during the freezing of the primary crystals is lighter than the initial composition of the melt. In turn, the melt convection redistributes the solute concentration in boundary layer and mushy zone leading to dramatic changes in growth rate and direction and may provoke the development of segregation freckles [5-12]. Further effects concern the selection of the secondary branches of growing dendrites [9]. In general, the flow

impact might be different for different regions of the mushy zone. The growth rate is increased by a removal of the solute, whereas an influx of solute-rich melt causes the formation of segregation freckles by a remelting of already solidified crystals.

Electromagnetic stirring by rotating or travelling magnetic fields can be used as an effective tool for flow control in solidifying metal alloys [6, 8, 13-18]. This research is also driven by the idea of a potential "repair" of the defects arising from the action of natural convection [6]. However, reaching this goal is not straightforward. By applying a traveling magnetic field Medina et al. [6] had to notice that the electromagnetic forces can control the positions of segregation channels and partly prevent the unsteadiness of buoyancy effects, but, they cannot fully eliminate the segregation effects.

It was shown recently, that the application of modulated AC magnetic fields offers considerable potential for optimizing the melt stirring [19-21]. Especially, the secondary flow can be organized in such a way that periodic reversals of the flow direction occur adjacent to the solidification front, which has been proven as an important method to achieve homogeneous, fine-grained, globular structures without flow-induced macrosegregation [18]. Moreover, it became apparent that a careful adjustment of the modulation parameters is required in order to create intense secondary flows with periodic reversals of the flow direction.

Nevertheless, the interaction between solidification and melt flow is rather complex and a further improvement of understanding the mechanisms is still needed. A better founded knowledge requires new diagnostic tools which allow *in-situ* observations of the process and provide high resolution data of the flow field, the concentration field and the solidified structure. Moreover, access to different length scales, as for example dendrite morphology and flow structure, is of particular interest.

During the last two decades new X-ray sources and innovative procedures for image analysis have dramatically improved the capabilities for visualization of solidification processes in metallic alloys [22-26]. The X-ray radiography technique enables real-time and *in-situ* observations of the solidification front with a spatial resolution of a few microns. For instance, Koster et al. [23] employed X-ray radioscopy for the investigation of melt convection effects in liquid Gallium - Indium alloys. Besides a reconstruction of the phase distribution inside the sample they demonstrated the capability to reproduce temperature fields and qualitative flow patterns. Shevchenko et al. [11] have shown that the occurrence of different segregation structures can be attributed to the occurrence of different patterns of melt convection adjacent to the solidification front and in the interdendritic region of the upper mushy zone.

The project "Magnetic Flow Control Solidification" of the Helmholtz Alliance "LIMTECH" was a collaborative work between ACCESS e.V., the Technical University Dresden (TUD) and the Helmholtz-Zentrum Dresden-Rossendorf (HZDR) and focused on the effects of melt convection on dendritic growth and on the question of whether effective control of microstructure formation can be achieved with the elaborate application of electromagnetic fields. The project should deliver substantial contributions for the development of innovative technologies to achieve casting products with superior mechanical properties. Solidification experiments have been conducted in Al-Cu and Ga-In alloys. Corresponding numerical simulations investigated the impact of diverse temperature and concentration fields on the morphology of dendritic structures. This article gives an overview of the main research activities in this project and is composed as follows: section 2 describes the experimental setups used by ACCESS and HZDR and gives a short description of the numerical scheme developed by TUD. Two phenomena formed the focus of the investigations, the fragmentation of primary dendrites and the development of segregation structures, since both processes have a significant influence on the mechanical properties of the solidified alloy. The fragmentation is the subject of section 3. Results from solidification experiments in Al-10wt%Cu and Ga-25wt%In are presented here. A numerical model was developed which is able to predict the fragmentation of dendrite sidearms during coarsening. This model was successfully validated with experimental results from studies on the coarsening behavior of Ga-In alloys. The role of natural convection on the formation of segregation freckles is considered in section 4, while the influence of an electromagnetically driven convection on fragmentation and segregation is discussed in section 5.

2. Experimental methods

This section describes the experimental setup and methods used by the partners ACCESS and HZDR. While the experiments performed by ACCESS considered the solidification behavior of non-refined and refined Al-10wt%Cu alloys, the activities by HZDR were exclusively focused on solidification experiments using Ga-In alloys.

2.1. ACCESS

Al-Cu samples were prepared from high-purity Al and Cu and were cast in rod-like steel moulds according to a final composition of Al-10.0 wt%Cu. For directional solidification experiments, cylindrical samples with a diameter of 8 mm and a length of 200 mm were processed using a Bridgman-Stockbarger furnace (see figure 1a) in an argon atmosphere. The samples were directionally solidified at a temperature gradient of 10 K/mm. Different velocities between 8.3 µm/s and 167 µm/s were adjusted by moving the furnace vertically upwards along the sample.

In-situ observations were realized in a quasi 2D setup using sheet-like samples of 50 mm in length, 5 mm in width and 150 µm in thickness. These samples were integrated in another Bridgman-Stockbarger type furnace. The corresponding setup is shown in the figures 1b and 1c. A temperature gradient along the sample of 11 K/mm was imposed by two heaters separated by an adiabatic gap. Directional solidification was controlled by a relative vertical motion of the sample with respect to the furnace using a stepping motor. The whole setup is mounted on a support structure between an X-ray source and an X-ray detector. A magnification of about 5 was chosen which provides a field of view of about 5 x 5 mm^2. That way, *in-situ* and real-time observation of the solidification process is realized with an acquisition rate of 1 frame every 2s and an effective pixel size of about 2 µm at the CCD sensor. More details of the experimental set-up are given in [27].

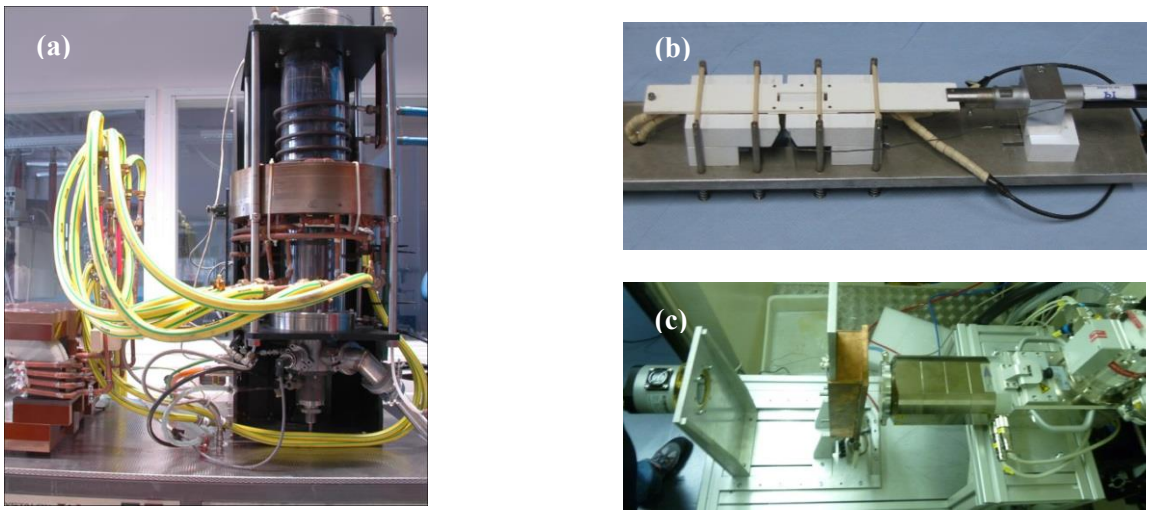

Figure 1. Scheme of the experimental setup at ACCESS: (a) Bridgman gradient furnace, (b) sample, integrated into a sample holder and adapted to the micro-Bridgman furnace unit (left) with linear actuator (right), (c) X-ray tube (right), micro-Bridgman furnace with active cooling in the copper housing (center) and CCD radiation detector (left).

2.2. X-ray laboratory at HZDR

A microfocus X-ray tube (XS225D from Phoenix|X-ray) was used for the solidification experiments carried out at Helmholtz-Zentrum Dresden-Rossendorf. The detailed description of the experimental setup can be found in [11, 28]. The majority of experiments was performed with a Ga–25wt%In alloy ($T_{Liquidus}$=25 °C, $T_{Solidus}$=15.3 °C) which was prepared from high-purity Ga (99.99%) and In (99.99%). It was melted in an furnace and filled into a 30 × 30 mm^2 Hele-Shaw quartz cell having a 150 µm gap parallel with respect to the direction of the X-ray beam (see figure 2a). The observation window was

approximately 9 × 12 mm^2. The images were captured with a scan rate of 50 half frames per second and integrated over a period of 1 s to reduce the noise level of single images. The tube voltage was 63 kV and the electrical current was 140 µA. The solidification cell was positioned between X-ray tube and detector as demonstrated in figure 2b. A linear array of Peltier elements on the lower edge of the solidification cell is operated as cooler. A simultaneous regulation of the Peltier cooler and the electric heater mounted at the upper part of the solidification cell enables controlling of the cooling rate and the temperature gradient across the cell during the experiment. A set of miniature K-type thermocouples were contacted to the outer surface of the cell to monitor the temperature. The electromagnetically driven flow was generated by a pumping device, which is represented by a rotating wheel consisting of two parallel discs with a set of permanent magnets (NdFeB) with alternating polarization at their inner sides. The top part of the solidification cell was placed between the disks. Rotation speeds of 30 and 80 revolutions per minute (rpm) were chosen for the magnetic wheel.

The analysis of the solidification front velocity and primary and secondary arm spacing follows the algorithm proposed by Boden et al. [29]. The concentration profiles were determined from the measurements of the local brightness in the images.

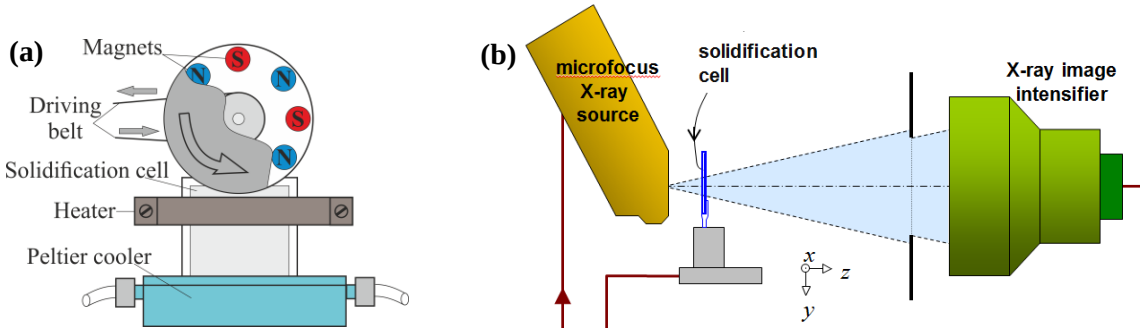

Figure 2. Experimental setup: (a) square Hele-Shaw solidification cell equipped with electric heater, Peltier elements and magnetic wheel for generation of the melt flow; (b) X-ray diagnostic system.

2.3. Beam-line ROBL at ESFR

Further visualization experiments were performed at the ROBL beam line (BM20) at the ESRF in Grenoble. The solidification cells used here for the solidification experiments were the same as already been employed for radiographic investigations carried out by means of a microfocus X-ray tube and described in the previous subsection. The solidification cell was exposed to a monochromatic X-ray beam characterized by an energy of 28.5 keV. Conventional transmission radiographs were obtained by means of a scintillator which provides a resolution of 2 µm. Further components for image acquisition were an optical magnifier and a PCO 2000 CCD camera with 2048 × 2048 pixels (pixel size: 0.34 × 0.34 µm^2). This equipment provides a field of view of about 700 × 700 µm². The distance between detector and sample was approximately 20 cm. In order to change the location of the observation window, the position of the solidification cell was manipulated with respect to the X-ray beam by a translation motor system with a minimal step < 10 µm. Images were acquired at exposure times ranging from 2 to 20 seconds. The exposure times were optimized in order to achieve an acceptable signal-to-noise ratio and a sufficient contrast for a specific process rate.

3. Fragmentation

The detachment of dendrite sidebranches is an important fragmentation mechanism and is considered as one of the major unresolved questions in the field of solidification. It is known that convection in a solidifying melt can promote the transition from a columnar to an equiaxed grain growth (CET). In particular, many studies have demonstrated that the application of electromagnetic stirring enhances the area of equiaxed grains and reduces the mean grain size (see e.g. [8, 14-17, 30-33]). It is widely

accepted that flow-induced grain refinement and the CET in metallic alloys is triggered by the appearance of additional dendrite fragments originating from the columnar front. The mechanism for grain multiplication by melt convection is supposed to be complex. Hellawell et al. [34] suggested a multi-stage process including the generation and the transport of the fragments from the interdendritic area into the liquid region. In case of sufficient undercooling the fragments can survive and grow. In situations where the density of the primary crystals is greater than that of the liquid phase, sedimentation of the fragments and finally the blockage of the columnar front occur, if a critical concentration of equiaxed grains has been reached. However, none of these stages is fully understood until now.

In particular, two questions are discussed intensively in the literature: i) which mechanism governs the detachment of fragments from the dendritic skeleton and ii) how do the fragments reach the region ahead of the solidification front. Both issues have been investigated within our project. In the next section we will introduce a new theoretical model for improving the understanding of the dynamics of the pinch-off of dendritic side arms. This model was calibrated and validated by experiments performed at the ESRF synchrotron X-ray source in Grenoble (ROBL beamline, see section 3.2). Section 3.3 reports about experimental investigations carried out at ACCESS for studying the fragmentation in Al-10wt%Cu alloys during directional solidification.

3.1. Numerical sidearm model

A numerical model was developed within this project for predicting the evolution of important geometrical features of dendritic sidearms during coarsening and investigating the systematic effects of the cooling rate and basic geometrical parameters. The methodology which is described in [35] incorporates an axisymmetric phase-field model for capillarity-driven interface dynamics in a binary alloy. The model assumes the usual conditions for coarsening at vanishing melt undercooling where material transport is due to quasi-stationary diffusion through the liquid phase. In addition to the isothermal case, the effect of finite cooling rates is studied, where the solid volume varies over time.

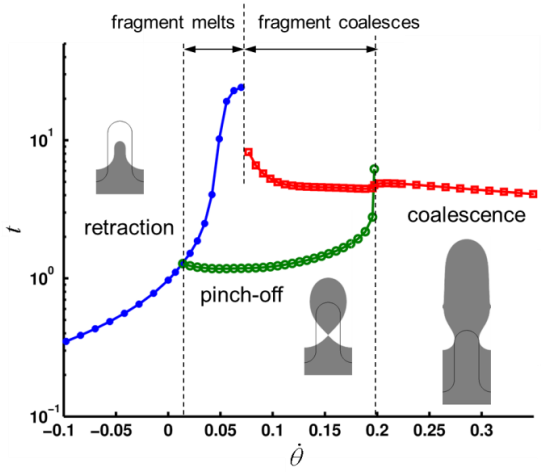

Figure 3. Durations of the different sidearm evolution scenarios as a function of cooling rate for some selected configuration; the initial and final evolution states are indicated by black and grey shapes respectively; all quantities are non-dimensionalized (for further details, see [35]).

The model was used to derive fundamental characteristics and limits of the pinching instability at the junction between a sidearm and its parent stem. It was shown that the evolution of the neck approaches the universal dynamics described in [36]. Moreover, the calculations revealed that the sidearm evolution is governed by its initial geometry and the rate of solidification. The durations and occurrence of different evolution scenarios, such as retraction or pinch-off, are shown in figure 3 as a function of the cooling rate. These results indicate that pinch-off only can only occur within a limited

range of cooling rates and is in competition with retraction and coalescence. For further details we refer the reader to [35]. An application of the model to experimental data and quantitative comparison can be found in [38].

3.2. Fragmentation experiments at ROBL

The solidification experiments for validation of the sidearm model were conducted in two stages:

- Growth stage: The Ga–25wt%In alloy was cooled down over a period of 30 min at a cooling rate of 0.01 K/s. The cooling phase is dominated by dendritic growth.
- Isothermal stage: After completion of the cooling phase an isothermal state was maintained over a period of 150 min retaining a constant temperature difference of 15 °C between heater and cooler. The coarsening of the dendrite structure occurs during this stage.

For studying the temporal evolution of the side arm morphology during the isothermal holding stage we selected an observation window which is centered 6.5 mm above the bottom cooler (see figure 4). Figure 5a-c shows an enlarged image segment of figure 4. Here, the brightness gradients are plotted for a better identification of the contours of the solid structure. The picture sequence illustrates the evolution of the shape of the three sidearms (labelled 1, 2, 3) during the pinch-off process. The narrow neck is formed above the junction between the sidearm and the parent stem. Later, the sidearm 2 detaches at the neck and the resulting fragment coarsens into a spheroid (figure 5c).

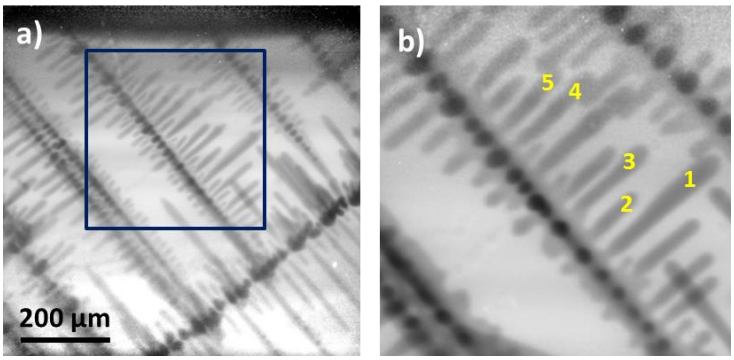

Figure 4. X-ray images showing the area of investigation: (a) dendritic structure with field of examination (blue box), (b) dendrite with five sidearms selected for quantitative measurements.

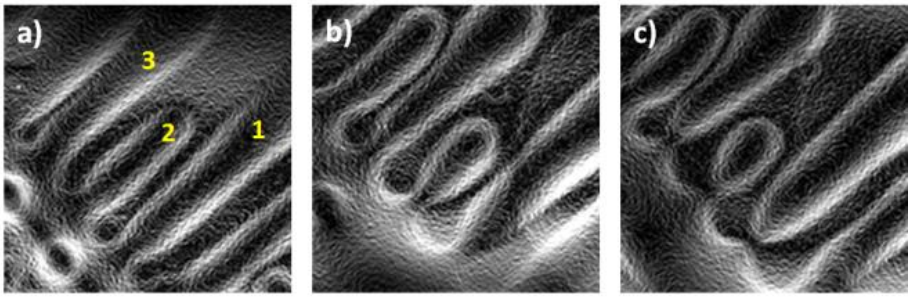

Figure 5. Images showing the development of secondary branches at different times during isothermal coarsening: (a) 5380 s, (b) 1670 s before- and (c) at the moment of pinch-off.

Measured values for the neck diameter as a function of time obtained from image processing are presented in figure 6. The same behavior of the neck diameter can be observed for all five side arms presented here. It shows the typical dynamics of capillarity-driven pinch-off, where the neck approaches a self-similar state during collapse [36]. The reduction of the neck follows the expected

$t^{1/3}$-law. Measurement uncertainties are responsible for the stronger decline of the neck diameter just before the pinch off. Likewise, the scatter of the data is caused by the limited contrast and image noise.

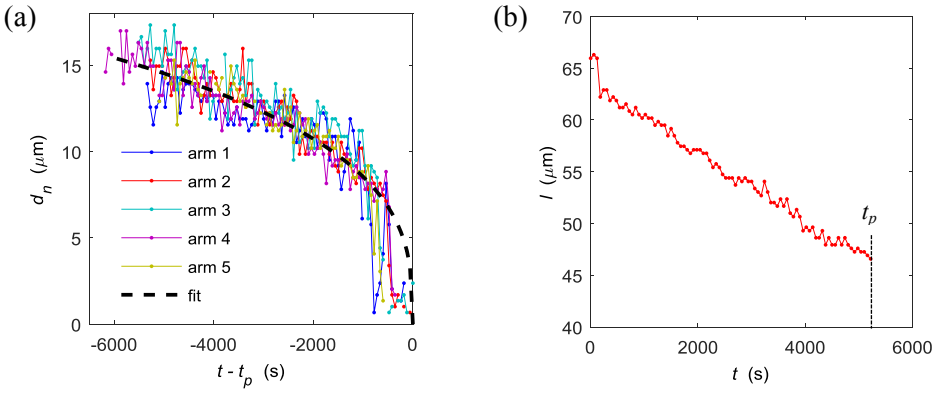

Figure 6. (a) Evolution of neck diameter for the sidearms labeled in figure 4b; the data is fitted to the pinching model in [36], where t_p is the pinch-off time. (b) Evolution of the length of the sidearm 2.

We demonstrate in [38] that the measured dynamics can be reproduced very well by means of numerical simulations using the axisymmetric sidearm model presented in the previous section. The corresponding temporal dynamics of the pinching processes have been utilized for determining the parameter Dd_0 (diffusion coefficient multiplied by the capillary length), which is a parameter of primary interest in modelling solidification and coarsening processes. This procedure has the potential to quantify the value for Dd_0 by *in-situ* observations followed by a rather simple theoretical analysis, which otherwise needs to be acquired from various delicate experiments.

3.3. Fragmentation in Al-10wt%Cu alloys

A series of solidification experiments investigated the formation of the grain structure in Al-10wt%Cu alloy during directional solidification. The experiments were carried out at ACCESS both in 3D bulk samples and in 2D sheet-like samples for visualization of grain growth and fragmentation using *in-situ* X-ray diagnostics. The specific alloy composition was chosen because of its special property that both the initial melt composition and the solidifying primary Al dendrites have almost identical densities. Therefore, gravity-related effects such as buoyancy or sedimentation acting on nucleated or fragmented solid particles in the melt are expected to be negligible.

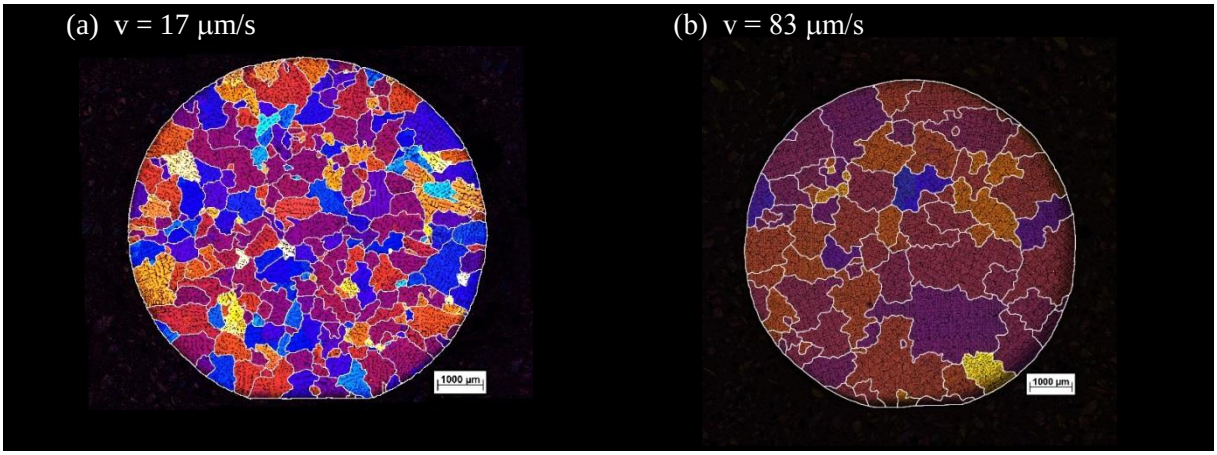

Figure 7. Grain structure in radial cross-section of the processed sample; the colors refer to the grain orientation.

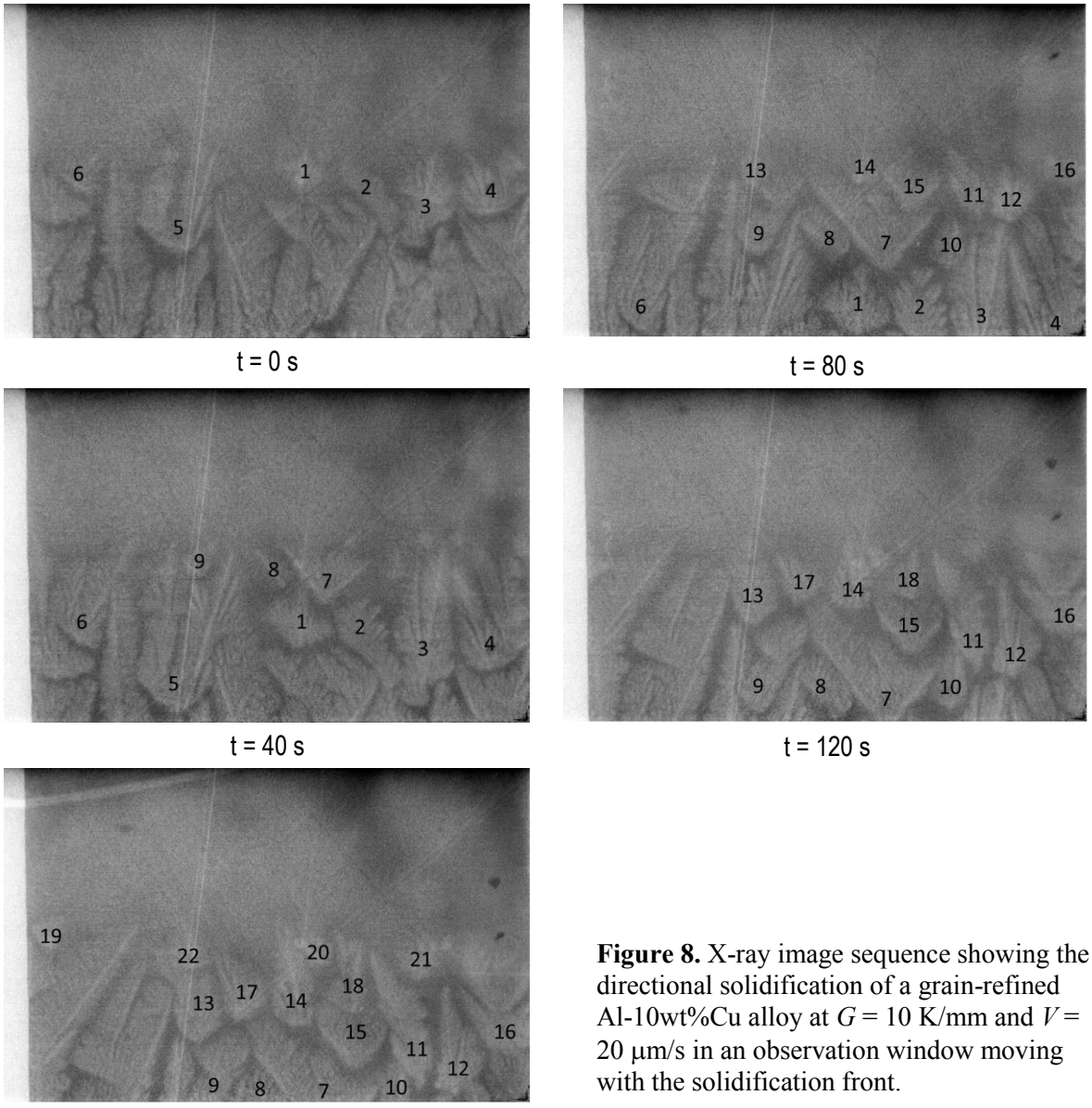

Figure 8. X-ray image sequence showing the directional solidification of a grain-refined Al-10wt%Cu alloy at G = 10 K/mm and V = 20 μm/s in an observation window moving with the solidification front.

The main result is that unexpected growth of equiaxed grains was found at low solidification velocities where normally columnar growth would be expected. By contrast we found that more columnar grains occur for higher solidification velocities (see [27] for details). Exemplary grain structures in radial cross-sections for different solidification velocities are presented in figure 7. For the lowest velocity many grains exist with different orientations (represented by the wide spectrum of different colors), whereas for higher velocities larger grains appear with a preferred orientation, see the narrower color spectrum compared to figure 7a. This surprising result can be explained by fragmentation. In-situ X-ray observations revealed that fragments continuously detach from the dendrite tip region. Within the solutal boundary layer at the solid-liquid interface they experience a moderate acceleration due to the higher solute concentration. If the resulting velocity of the fragments is larger than that of the solidification front, the fragments growing in the interdendritic liquid can leave the mushy zone. Buoyancy disappears as a driver for the motion of the fragments as soon as a fragment has left the solutal boundary layer. The fragments stay just ahead of the columnar front and form new equiaxed grains in the undercooled region [27]. This is the reason why the equiaxed grain

structure appears at low solidification velocities, which is normally expected for much higher solidification velocities due to the classical columnar-to-equiaxed transition (CET).

Further solidification experiments were carried out in refined alloys. Here, 0.1wt%Al-Ti-B was added as grain refiner to the Al-10wt%Cu alloy. Directional solidification was achieved applying a temperature gradient of 10 K/mm and a solidification velocity of 20 μm/s. The results were compared to corresponding data obtained from non-refined alloys [27]. An exemplary sequence of images recorded at a time interval of 20 s is displayed in figure 8. Here, an ascending numbering of the grains was inserted for better identification. It can be seen that new grains are constantly being formed and that these grow subsequently. A fragment is usually the nucleus of the new grain. It is difficult to answer whether additional crystal nuclei are formed in the subcooled melt due to grain refinement. In order to detect such nuclei in their initial growth phase, the local and temporal resolution of the X-ray diagnostics used is not sufficient.

The nucleation rate can be estimated from figure 8. In the time interval t = 40 s to t = 140 s, about 15 new nuclei are produced (8 to 22). The respective nucleation rate of 0.15 nuclei/s is only slightly higher than that in non-grain refined alloy with 0.10 nuclei/s [27]. Thus, it can be concluded that fragmentation occurs in grain-refined as well as in non-grain-refined Al-10%wtCu alloys for the solidification parameters given here, and results in the same nucleation rates. Thus, the grain refining agent is not capable of sufficiently reducing the critical nucleation undercooling in order to generate further grains. As in the case of the non-grain-refined alloy, the vertical component of the buoyancy rate of the fragments is also estimated here before they are trapped by the solidification front. A movement of around 550 μm in a time interval of 40 s is typical. This means that an average buoyancy speed of about 14 μm/s can be determined. This value agrees very well with the value for the non-grain-refined alloy, which was between 10 μm/s and 16 μm/s. Thus, both alloys are not different in terms of fragmentation behavior.

4. Segregation

Thermosolutal convection has been identified as the main reason for the development of solute-rich channels in the mushy zone during the solidification of metallic alloys. The development of such kind of segregation channels was studied by means of X-ray radioscopy using the setup described in section 2.2. The Ga–25wt%In alloy was solidified directionally in vertical direction from the bottom of the solidification cell. Figure 9 presents a series of images documenting an exemplary solidification process. The solidification of this alloy composition leads to a growth of In dendrites. The restricted solubility of Ga in the In primary crystals causes an accumulation of rejected Ga and a formation of a solutal boundary layer as shown in figure 9a. The gallium-enriched melt is less dense as compared to the initial composition. Due to the unstable density stratification an intense solutal-driven convection occurs in form of rising plumes containing Ga-rich liquid. As a result, an arrangement of convection rolls is formed along the solidification front (see figure 9b). Further solute accumulation in the upper mushy zone intensifies the solutal convection. Figure 9c illustrates the formation of distinct plumes, whose intensity and lifetime are determined by the extent to which the plume can be fed by new Ga-rich melt in the mushy zone. Due to the continuity condition, the roll structures at the solidification front induce a convective transport of In-rich fluid towards the mushy zone, which promotes the growth of the dendrites at the edge of the plumes. The resulting solute is carried by the flow into the region below the ascending plume. The increasing Ga concentration lowers the local melting temperature and causes an inhibition of dendritic growth and even a re-melting of solid material. Finally, a segregation freckle (chimney) originates (see figures 9c and 9d). The flow structures observed in our experiments reveal a transient behavior. Parameters like the intensity and the position of the plumes are not constant over time. The unstable flow obviously affects the development of the segregation chimneys. A perturbation of the ascending plume appears in figure 9d. This enables the inflow of In-rich melt into the chimney (figure 9e) which results in an accelerated crystal growth. The consequence is a “self-healing” process, i.e. the chimney is filled in a short time by new dendrites and finally disappears (figure 9f).

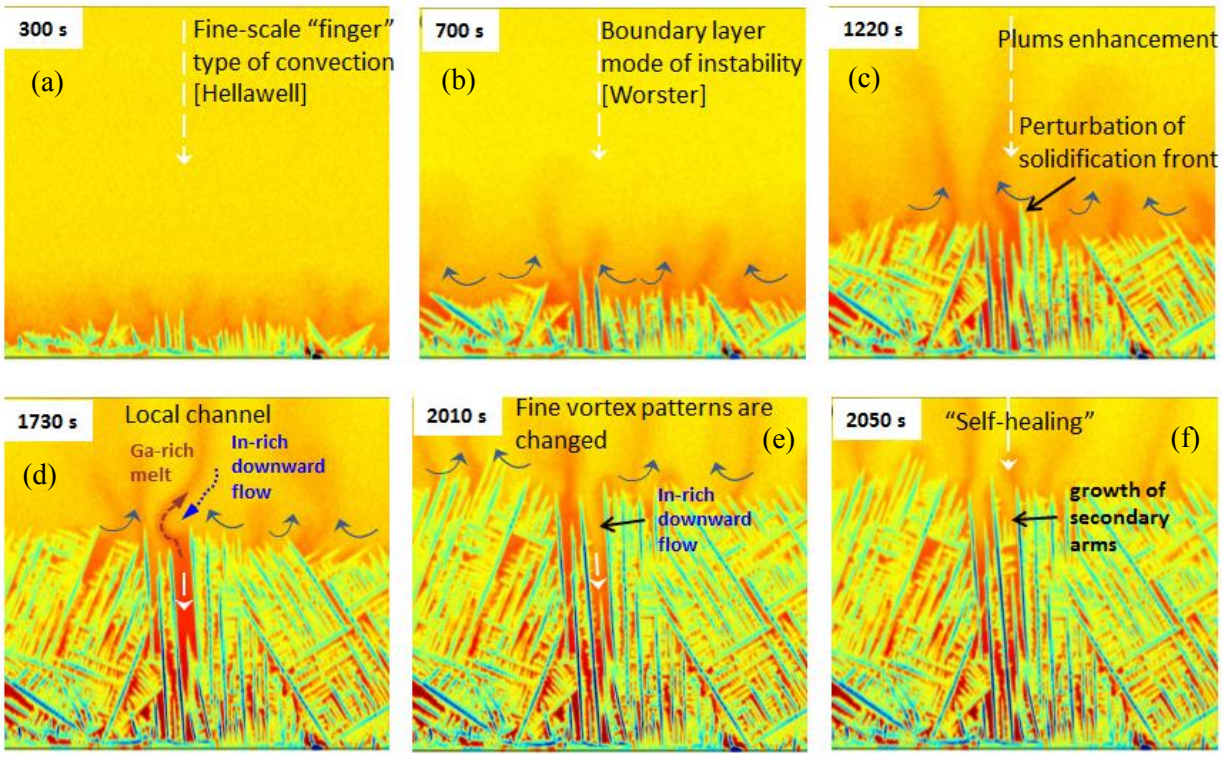

Figure 9. X-ray visualization showing an exemplary bottom-up solidification of a Ga-25wt%In alloy. The color scale represents the Ga concentration (red – Ga-rich melt, blue/green In dendrites).

The behavior described above raises the question how many of the emerging chimneys will survive and can be found in the solidified material. The long-term stability of these segregation channels and the role of the solute Rayleigh number in this context were investigated in [11]. This study showed that different segregation structures occur due to variations of the temperature gradients which in turn cause modifications of the melt flow pattern. While the stability of the chimneys is very much subject to fluctuations in the flow structure in case of low temperature gradients, the situation at higher temperature gradients is characterized by two dominating convection rolls in the liquid phase which are driven by a lateral temperature gradient and the convex shape of the solidification front. This configuration induces a continuous accumulation of solute in certain regions of the mushy zone and promotes the development of sustaining chimneys. The experimental data obtained by the X-ray radiography were also used for the validation of corresponding numerical simulations [12]. Both simulation and experiment show the complex interaction between the flow structure and the solidification dynamics. For instance, a "pulsing" behavior of the plumes and the occurrence of solute-enriched zones in the upper mushy zone beneath dominating plumes were found. Moreover, a 3-D model of freckle formation at a microstructural level was coupled with in the *in-situ* X-ray radiography to predict the mechanisms of freckle initiation and growth [37].

5. Electromagnetic stirring

5.1. Solidification of Al-10wt%Cu alloys under the influence of an RMF

Another series of solidification experiments were performed at ACCESS where a rotating magnetic field was additionally incorporated at the gradient furnace. Three coil pairs are dimensioned in such a way that homogeneous field strength is ensured over a height of 10 cm. The coil system is moved along with the furnace so that the magnetic field during solidification is always effective in the region

of the solidification front. The frequency of the rotating magnetic field is constant at 50 Hz. The magnetic induction can be continuously adjusted from zero up to 13 mT allowing to generate a flow with different intensities in the solidifying melt. The experimental investigations were carried out for solidification velocities varying between 8.3 and 167 µm/s. Figure 10 compares cross sections of samples solidified at a solidification velocity of 16.7 µm/s and different magnetic field strengths of the RMF. At the solidification rate considered here the electromagnetically driven convection causes an increase of the number of grains. For the weaker excitation (B = 2 mT), the mean grain size and average grain size looks rather similar as without an external magnetic field. Based on the quite uniform color spectrum of the electrolytically etched sections for B = 2 mT we can infer small differences in the orientation of the dendrites. This is presumably due to the fact that the slow flow homogenizes the melt and promotes the growth of a few well-directed grains. The stronger excitation (B = 10 mT) generally leads to a clear increase in the mean grain count, as well as a correlation with a decrease in average grain size.

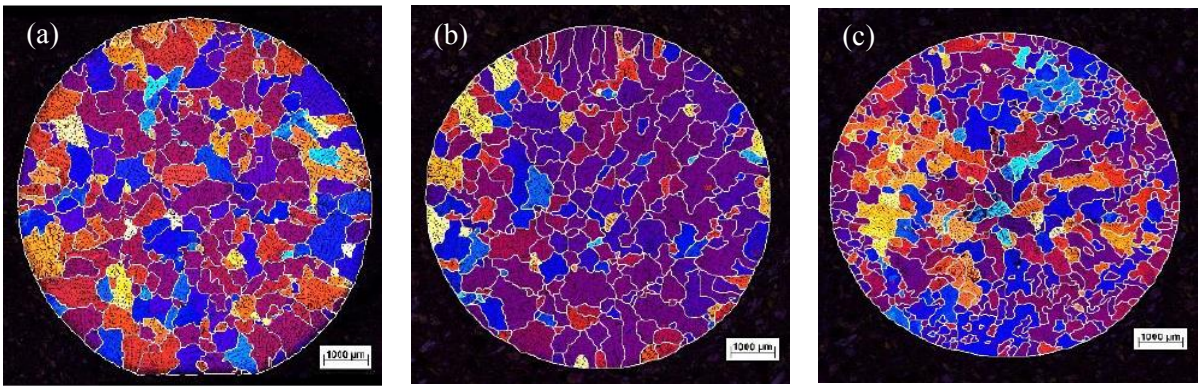

Figure 10. Cross sections of the samples solidified at V = 16.7 µm/s revealing the grain structure: (a) B = 0, (b) B = 2 mT, (c) B = 10 mT.

In general, in the case of low solidification rates (V = 16.7 µm/s), fragmentation seems to play the decisive role. Almost independently of the intensity of the flow in the melt, new grains are formed, which are rapidly overgrown by neighboring grains. Intensive flow leads to a growth of inclined grains, while an equiaxial grain structure remains predominant. With increasing solidification rates - starting at about 50 µm/s - a columnar grain structure predominantly forms. The number of grains decreases and the mean grain size increases. This effect occurs in the case of no induced flow (B = 0) and weak forced convection (B = 2 mT). With intensive flow (B = 10 mT) one finds many, often obliquely growing grains.

5.2. Visualization of the effect of electromagnetically driven convection by X-ray radiography

The X-ray radiography was used for an *in-situ* study of the effect of electromagnetic stirring during the solidification of a Ga-25wt%In alloy in a Hele-Shaw cell. The experimental setup was the same as in Chapter 4. The equipment was extended by a magnetic wheel, which allowed for a controlled excitation of a melt flow in the liquid phase.

Figure 11 shows a sequence of images demonstrating a growth process of In dendrites captured at different times. The development of ensembles of dendrites with different orientations is caused by the fact that no special preparations were made to control the nucleation at the bottom of the solidification cell. The effect of natural convection becomes obvious in figure 11a showing the situation before the magnetic wheel was switched on. Distinct solutal plumes dominate which are ejected at the solid-liquid interface since their density is lower compared with the bulk melt. The rising plumes are accompanied by a downward flow of In-rich melt in the intermediate regions. Accordingly,

measurements of the local Ga concentration presented in figure 12a reveal an inhomogeneous horizontal concentration profile along the solidification front. Figures 11b and 11c are recorded at two different times after the magnetic wheel started to rotate counter-clockwise with 30 rpm (rotation per minute). The resulting induced flow is almost horizontal with respect to the solidification front with a velocity of about 0.3 mm/s.

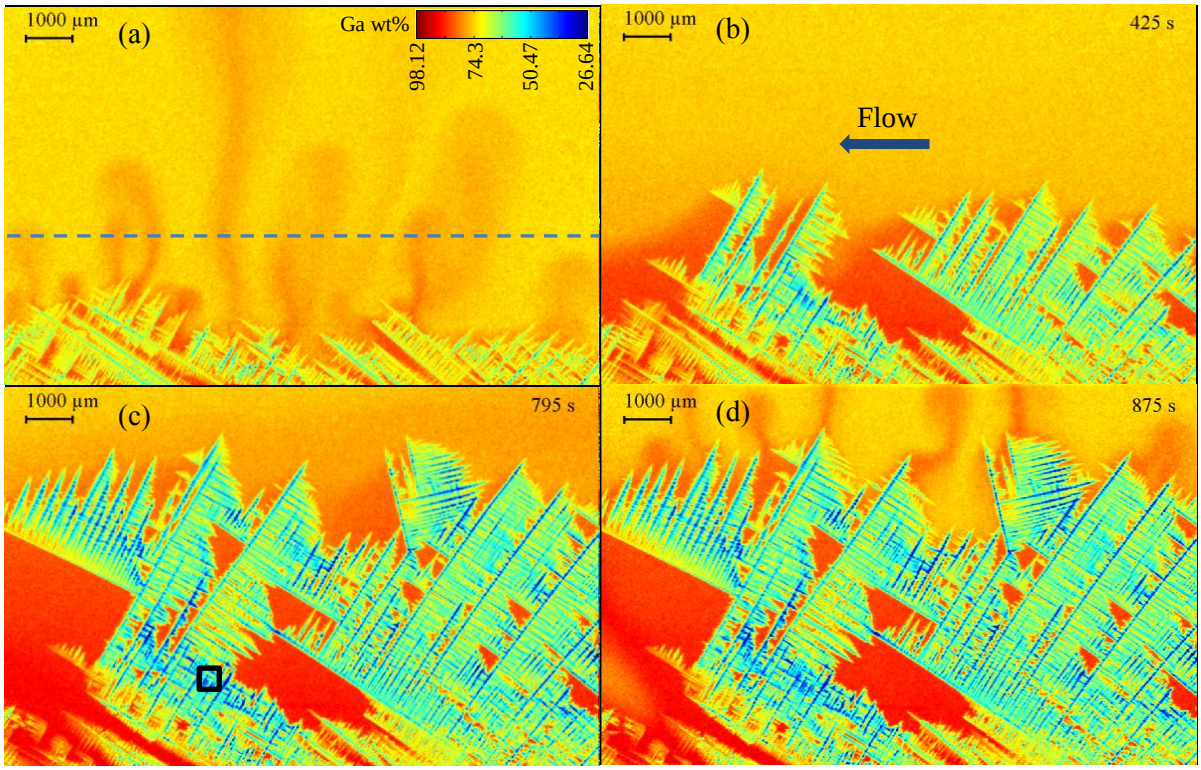

Figure 11. Image sequence showing the solidification of the Ga - 25wt%In alloy under the influence of forced convection at different times: (a) 155 s, (b) 425 s, (c) 795 s and (d) 875 s. Rotation rate of the magnetic wheel was 30 rpm.

In case of forced convection the solutal plumes are strongly damped and the final concentration profile along the solidification front becomes smooth (see the red curve in figure 12a). Slight increase of the Ga concentration on the left-hand side of the red curve is caused by blurred plumes running along the solidification front from right to left. The velocity of the solidification front decreases gradually from ~ 12.9 µm/s down to ~ 4.5 µm/s during its exposure to the driven flow (see figure 12b). This can be explained by a continuous increase of Ga concentration near the solidification front with progressing exposure time.

Another interesting effect can be observed during solidification: the uneven growth of primary dendrites at the beginning of the experiment leads to the formation of Ga-rich zones near the solidification front which develop into distinct segregation freckles as it can be seen on the left-hand side of figures 11b and 11c. Moreover, a competitive growth between secondary branches and primary dendrites leads to an increase of the primary arm spacing. Preferential growth of the secondary arms is observed at the upstream side of the dendrites. In contrast, high solute concentration at the downstream side strongly influences the formation of secondary arms: in case when dendrites are inclined against the upcoming flow the secondary arms at the downstream side are fully eliminated; in case when the dendrites are inclined towards the upcoming flow only few secondary arms develop and create tertiary arms. Furthermore, the inclination angles of the growing dendrites change by several

degrees under the influence of the forced flow. A short time after the magnetic wheel is switched off the solute plumes re-appear (see figure 11d) and the solidification velocity increases again (see figure 12b).

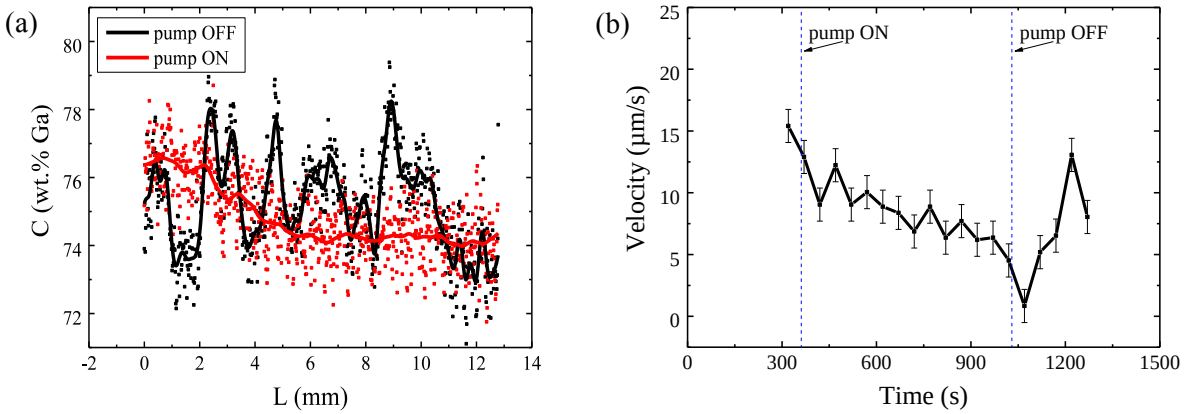

Figure 12. (a) Concentration profiles along the solidification front: 10 s before (black line) and 30 s after (red line) the initiation of the magnetic wheel. Measurements were carried out along the dashed line highlighted in figure 11a. (b) Velocity of the solidification front. The rotation rate of the magnetic wheel was 30 rpm.

Figure 13 shows another experiment carried out at a higher rotation rate (80 rpm, clockwise direction). The situation in figure 13a corresponds to the initial phase of the experiment when the magnetic wheel remains idle. As in the previous experiment the plumes are completely suppressed once the rotating magnetic wheel induces a significant forced flow (figures 13b and 13c). Figure 14a shows the corresponding Ga concentration profiles before (black) and after (red) the magnetic wheel was switched on. It can be seen that the forced flow straightens the Ga concentration along the solidification front considerably. The growth velocity of the solidification front decreases from a value of ~ 14.2 µm/s down to ~ 2.5 µm/s (see figure 14b). Such a fast and strong decrease can be explained by the accumulation of Ga-rich solute with time near the solidification front. A pronounced Ga-rich layer develops near the solidification front due to uneven growth of dendrites (see figure 13c). This leads to the evolution of distinct segregation freckles (see the right-hand side of figures 13b and 13c). The induced strong flow turns out to be an efficient carrier of In-rich material promoting the dendrite growth. As a result secondary arms grow preferably at the upstream side of the dendrites; while their development is impeded at the downstream side due to the high solute concentration. Increasing arm spacing due to competitive growth between secondary and primary arms is also observed. As in the previous experiment, the solute plumes re-appear again after the magnetic wheel is switched off (see Figure 13d).

Despite multiple similarities certain differences between the two experiments can be clearly identified: first, regions with higher In concentration are built up at higher rotation speeds (80 rpm) (see figures 11c and 13c for comparison). The average In concentration was measured in both experiments in the most In-rich areas marked as squares in the figures 11c and 13c (0.52×0.52 mm^2 size). A value of ~ 47.5wt% was found for 30 rpm, while a value of ~ 63.6wt% occurs in the second experiment at 80 rpm. Moreover, the effects of the reduction of the solidification front velocity and the flattening of the concentration profiles along the solidification front appear to be much stronger in case of the more intense forced flow.

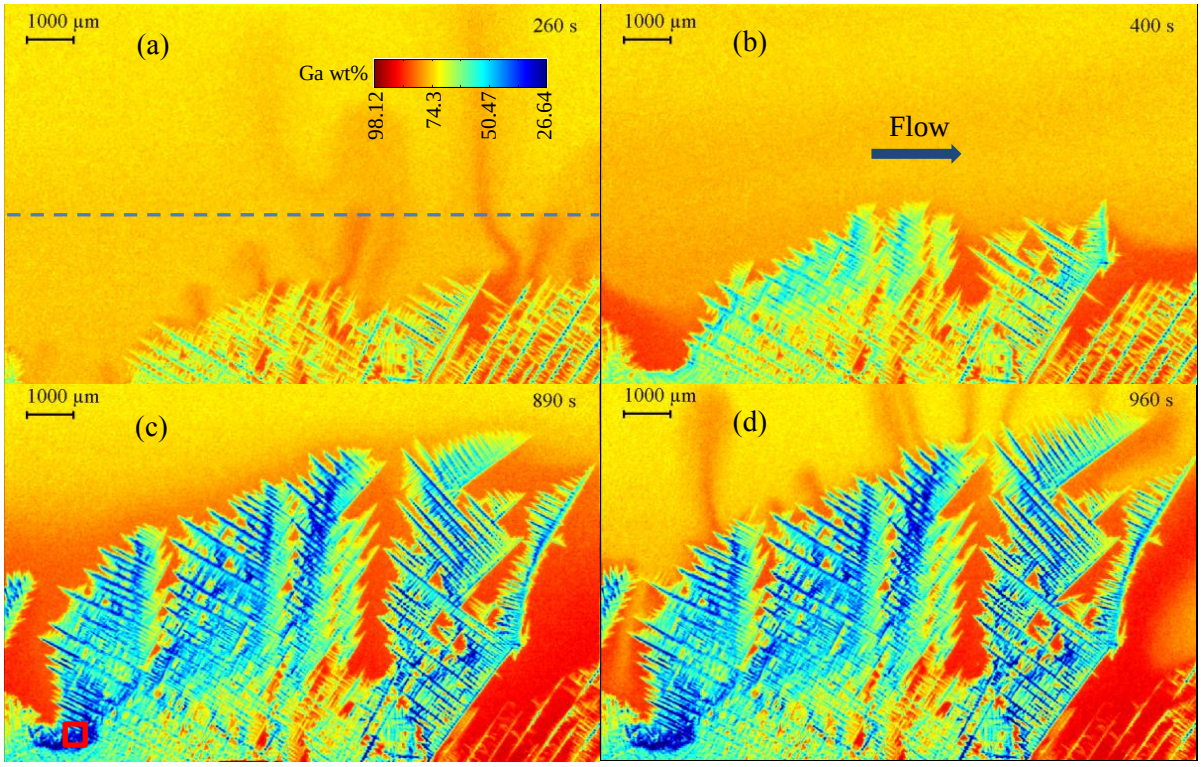

Figure 13. Image sequence showing the solidification of the Ga - 25wt%In alloy under the influence of forced convection at different times: (a) 260 s, (b) 400 s, (c) 890 s and (d) 960 s. Rotation rate of the magnetic wheel was 80 rpm.

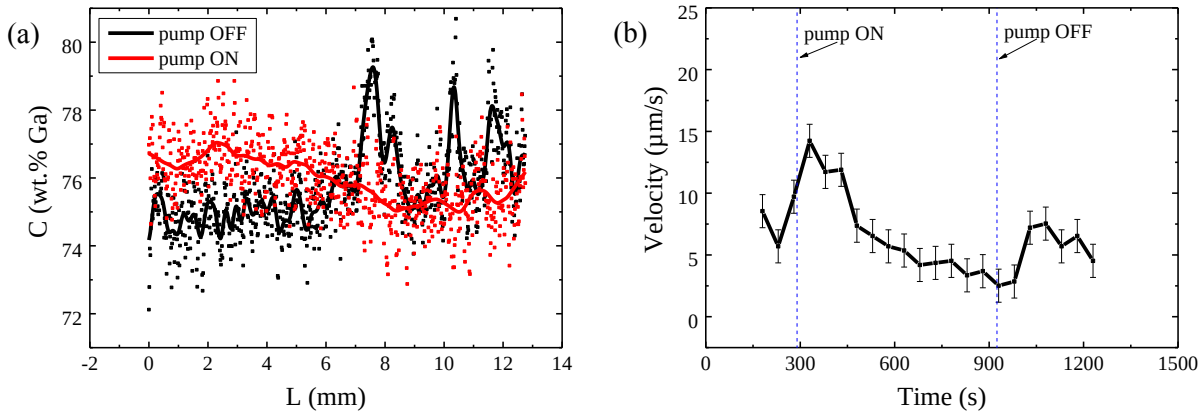

Figure 14. (a) Concentration profiles along the solidification front: 10 s before (black line) and 30 s after (red line) the initiation of the magnetic wheel. Measurements were carried out along the dashed line highlighted in figure 13a. (b) Velocity of the solidification front. The rotation rate of the magnetic wheel was 80 rpm.

6. Conclusions

We have presented experimental and numerical results that were obtained within the project "Magnetic Flow Control Solidification" of the Helmholtz Alliance "LIMTECH". The main goal of the project was to improve the understanding of the complex interactions between melt flow and solidification. In particular we have addressed several aspects in the context of grain refinement, dendrite fragmentation and segregation mechanisms. Various solidification experiments were

performed for studying solidification processes under the influence of natural convection or electromagnetically driven flow. Directional solidification experiments with an Al-10wt%Cu alloy have revealed an unexpected equiaxed grain growth at low solidification velocities, instead of columnar growth. This exceptional behavior was conclusively explained by the specific conditions that affect formation and movement of dendrite fragments at the solidification front. Further activities have focused on the evolution of dendritic structures during coarsening. The combination of theoretical modeling and experiments performed at the ESFR synchrotron X-ray source in Grenoble has allowed to improve the understanding of the pinch-off of dendritic side arms and to obtain material information that is relevant for quantitative modeling. Our future work will include the systematic study of the evolution of dendritic morphologies at finite cooling rates and under the impact of melt flow.

Acknowledgements
The authors acknowledge the financial support by the German Helmholtz Association in form of the Helmholtz-Alliance "LIMTECH". The authors also gratefully acknowledge the Rossendorf Beam Line (material research) at ESRF (Grenoble, France) and the scientific and experimental support from Joerg Grenzer, Olga Keplinger and Carsten Baehtz.

References
[1] Hellawell A, Sarazin J R and Steube R S 1993 *Philosophical Transactions: Physical Sciences and Engineering* **345** 507
[2] Sample A K and Hellawell A 1984 *Metallurgical Transactions A* **15** 2163
[3] Tewari S N and Shah R 1992 *Metallurgical Transactions A* **23** 3383
[4] Bergman M I, Fearn D R, Bloxham J and Shannon M C 1997 *Metallurgical and Materials Transactions A* **28** 859
[5] Murakami K, Fujiyama T, Koike A and Okamoto T 1983 *Acta Metallurgica* **31** 1425
[6] Medina M, Du Terrail Y, Durand F and Fautrelle Y 2004 *Metallurgical and Materials Transactions B* **35** 743
[7] Boden S, Eckert S and G Gerbeth 2010 *Materials Letters* **64** 1340
[8] Willers B, Eckert S, Michel U, Haase I and Zouhar G 2005 *Materials Science and Engineering A* **402** 55
[9] Steinbach S and Ratke L 2007 *Metallurgical and Materials Transactions A* **38** 1388
[10] Zimmermann G, Weiss A and Mbaya Z 2005 *Materials Science and Engineering A* **413-14** 236
[11] Shevchenko N, Boden S, Gerbeth G and Eckert S 2013 *Metallurgical and Materials Transactions A* **44** 3797
[12] Saad A, Gandin C A, Bellet M, Shevchenko N and Eckert S 2015 *Metallurgical and Materials Transactions A* **46** 4886
[13] Eckert S, Nikrityuk P A, Willers B, Räbiger D, Shevchenko N, Neumann-Heyme H, Travnikov V, Odenbach S, Voigt A and Eckert K 2013 *Eur. Phys. J. Spec. Top.* **220** 123
[14] Roplekar J and Dantzig J 2001 *International Journal of Cast Metals Research* **14** 79
[15] Griffiths W D and McCartney D G 1996 *Materials Science and Engineering A* **47** 46
[16] Kovács J, Roósz A and Szőke J 2006 *Materials Science Forum* **508** 263
[17] Zimmermann G, Vitusevych V T and Sturz L 2010 *Materials Science Forum* **649** 249
[18] Willers B, Eckert S, Nikrityuk P A, Räbiger D, Dong J, Eckert K and Gerbeth G 2008 *Metallurgical and Materials Transactions B* **39** 304
[19] Kojima S, Ohnishi T, Mori T, Shiwaku K, Wakasugi I and Ohgarni M 1983 *66th Steelmaking Conf. Atlanta, GA, ISS-AIME, Warrendale* 127
[20] Wang X, Fautrelle Y, Etay J and Moreau R 2009 *Metallurgical and Materials Transactions B* **40** 82
[21] Eckert S, Nikrityuk P A, Räbiger D, Eckert K and Gerbeth G 2007 *Metallurgical and*

Materials Transactions B **38** 977
[22] Mathiesen R H, Arnberg L, Mo F, Weitkamp T and Snigirev A 1999 *Phys. Rev. Lett.* **83** 5062
[23] Koster J N, Seidel T and Derebail R 1997 *Journal of Fluid Mechanics* **343** 29
[24] Reinhart G, Mangelinck-Noël N, Nguyen-Thi H, Schenk T, Gastaldi J, Billia B, Pino P, Härtwig J and Baruchel J 2005 *Materials Science and Engineering A* **413** 384
[25] Yasuda H, Ohnaka I, Kawasaki K, Sugiyama A, Ohmichi T, Iwane J and Umetani K 2004 *Journal of Crystal Growth* **262** 645
[26] Liotti E, Lui A, Vincent R, Kumar S, Guo Z, Connolley T, Dolbnya I P, Hart M, Arnberg L, Mathiesen R H and Grant P S 2014 *Acta Materialia* **70** 228
[27] Zimmermann G, Pickmann C, Hamacher M, Schaberger-Zimmermann E, Eckert K and Eckert S 2017 *Acta Materialia* **126** 236
[28] Shevchenko N, Roshchupkina O, Sokolova O and Eckert S 2015 *Journal of Crystal Growth* **417** 1
[29] Boden S, Willers B, Eckert S and Gerbeth G 2008 *Metallurgical and Materials Transactions A* **39** 613
[30] Johnston W C, Kotler G R, Ohara S, Ashcom H V and Tiller W A 1965 *AIME MET SOC TRANS* **233** 1856
[31] Vives C 1989 *Metallurgical and Materials Transactions B* **20** 623
[32] Campanella T, Charbon C and Rapaz M 2004 *Metallurgical and Materials Transactions A* **35** 3201
[33] Liu S F, Liu L Y and Kang L G 2008 *Journal of Alloys and Compounds* **450** 546
[34] Hellawell A, Liu S and Lu S Z 1997 *JOM* **49** 18
[35] Neumann-Heyme H, Eckert K and Beckermann C 2015 *Physical Review E* **92** 060401(R)
[36] Aagesen L K, Johnson A E, Fife J L, Voorhees P W, Miksis M J, Poulsen S O, Lauridsen E M, Marone F and Stampanoni M 2011 *Acta Materialia* **59** 4922
[37] Karagadde S, Yuan L, Shevchenko N, Eckert S, and Lee P D 2014 *Acta Materialia* **79** 168
[38] Shevchenko N, Neumann-Heyme H, Lei Z, Eckert K, Keplinger O, Grenzer J, Beckermann C and Eckert S 2017 *Acta Materialia (submitted)*